Progress In Electromagnetics Research M, Vol. 117, 139–150, 2023

A Design Method of Compact Metasurface-Based Dual-Band Planar Lens Antennas for Multibeam Applications

Shucheng Ni, Xiang-Qiang Li, Jinran Yin, Qingfeng Wang, and Jianqiong Zhang*

Abstract—A design method of compact dual-band multi-beam antennas is proposed by integrating a dual-band metasurface lens with a dual-band planar antenna array in this paper. The dual-band multi-beam antenna designed through this method has a compact configuration, low cost, and is easy to integrate with other devices for communication. The dual-band multi-beam function of the antenna by this method has been verified through a double-layer dual-band metasurface lens and a five-element dual-band planar antenna array. A dual-band meta-cell with relatively independent performance at 13 GHz and 23.5 GHz is designed to form the metasurface lens. Dual-band magnetoelectric (ME) dipole antenna is used as the feed antenna element. The simulated and tested results indicate that the lens antenna generates five independent beams at both 13 GHz and 23.5 GHz. Considering practical applications, solutions to improve antenna performance and reduce losses have also been proposed.

1. INTRODUCTION

In recent years, the vigorous development of wireless technology has driven researches on antenna technology. Technologies such as multi-band antennas, shared-aperture antennas, and multibeam antennas have been rapidly developed. Among them, multi-beam antennas are widely researched and applied in 5G wireless communications and satellite communications due to their unique coverage function. Multibeam antennas based on metasurface lens are attractive because of their low cost, compact structure, and simple signal processing methods [1].

Many researches on multibeam metasurface lens antenna have been reported. In [2], a thin planar lens antenna based on metamaterial working at 28 GHz is proposed for special beamforming and multibeam multiple-input multiple-output (MIMO). The antenna achieves a coverage of $\pm 27^\circ$ by using a dual-layer metasurface lens and seven feed antennas. The focusing characteristics under different ratios of focal length to aperture diameter are also studied. In order to further expand the phase shift range of the metasurface cell, the phase shift of more than 400° is realized by 180° phase reversals of the feed elements in [3]. By sacrificing the polarization in one direction of the metasurface cells through special design, the phase shift of more than 400° and the bandwidth of 15.7% are realized in [4]. In order to expand the coverage, some lenses that can realize wide-angle beam coverage are designed [5, 6]. Some planar Luneberg lenses have also been proposed as solutions for wide-angle beam coverage [7, 8]. When the application of metasurface lens expands to low frequency, the conventional electrically large lens is no longer suitable, and the lenses with relatively electric small size are proposed [9, 10]. In addition, some active lens antennas have also been proposed [11, 12]. Singleband metasurface lenses for multibeam applications have been widely reported.

Many dual-band metasurface lens antennas or transmitarrays have been researched. Most of the researches focus on dual-band lens antennas with fixed beam [13–16]. Some studies have considered dual-band beam scanning by offsetting the feed from the focus or rotatable transmitarray [17, 18]. The

Received 23 April 2023, Accepted 12 June 2023, Scheduled 28 June 2023
* Corresponding author: Jianqiong Zhang (qilinxing@163.com).
The authors are with the Southwest Jiaotong University, Chengdu, China.

dual-band rotatable transmitarrays are also proposed for dual-band beam scanning [19, 20]. In these researches, horn antennas are usually used as the feeds, which is not conducive to compact dual-band configuration and integrating with other devices. Compared with dual-band beam scanning with single feed at each band, the dual-band multi-beam function requires some dual-band feed elements to form an array, and each feed element needs to have a fixed position.

As a solution to the problem, a design method of compact dual-band multi-beam antennas by integrating a dual-band metasurface lens with a dual-band planar antenna array is proposed in this paper. The feasibility and mechanism of the method are discussed in Section 2. A dual-band meta-cell with relatively independent performance at 13 GHz and 23.5 GHz is designed, and the dual-band focusing characteristics are verified through a double-layer lens composed of the meta-cell in Section 3. A five-element dual-band planar antenna array is designed in Section 4. The double-layer dual-band metasurface lens integrated with the five-element dual-band planar antenna array is simulated, fabricated, and tested in Section 5, and the results indicate that the lens antenna generates five independent beams at both 13 GHz and 23.5 GHz. The dual-band multi-beam function can be achieved through this design method. The design method is suitable for applications with a frequency ratio close to 2. Considering practical applications, a method for greatly improving antenna performance is suggested.

2. MECHANISM AND DESIGN METHOD

The basic mechanism of lens antenna is to control the optical path or phase of electromagnetic wave, so that its wavefront can obtain the predetermined characteristics. Corresponding to the manipulation of path and phase, the lens forms are dielectric lenses and metasurface lenses, respectively. Dielectric lens controls the wavefront by using the path difference generated by the dielectric. Metasurface lenses use the phase shift characteristics of the metasurface to directly generate the phase difference, so as to control the wavefront. The monochromatic sine wave propagating forward along X axis of Cartesian coordinate system can be expressed as

$$E = E_0 \sin(\omega t - kx + \varphi) \tag{1}$$

where x and φ represent position and initial phase, respectively. If the path difference Δx and phase difference $\Delta\varphi$ are introduced, respectively, the formula will become

$$E = E_0 \sin(\omega t - k(x + \Delta x) + \varphi) \tag{2}$$

$$E = E_0 \sin(\omega t - kx + \varphi + \Delta x) \tag{3}$$

Due to the properties of trigonometric function, if

$$-k\Delta x = \Delta\varphi \pm 2n\pi \tag{4}$$

Δx and $\Delta\varphi$ will have the same effect on electromagnetic wave. The wavefront control effects of dielectric lens and metasurface lens with infinitesimal cells are equivalent. Therefore, the theories or conclusions of dielectric lens can be applied to the metasurface lens with infinitesimal cells to analyze its wavefront control characteristics. For the dielectric lens with a constant refractive index, the wavefront control effect is frequency independent. This is because the same path difference has the equivalent effect on far-field at any frequency. If Δx is used to replace $\Delta\varphi$, $\Delta\varphi$ can be expressed as

$$\Delta\varphi = -k\Delta x \pm 2n\pi = \frac{2\pi}{\lambda} \pm 2n\pi \tag{5}$$

Therefore, $\Delta\varphi$ depends on the wavelength λ and path difference Δx. For a certain Δx, the corresponding $\Delta\varphi_1$ and $\Delta\varphi_2$ can be calculated according to the corresponding wavelengths λ_1 and λ_2 at two different frequencies f_1 and f_2. Considering the frequency independent characteristics of dielectric lenses, $\Delta\varphi_1$ and $\Delta\varphi_2$ of the metasurface lenses will lead to the same effect at f_1 and f_2 for far-field electromagnetic wave.

In fact, infinitesimal metasurface cells cannot be achieved in practice. Usually, subwavelength metasurface cells are used to form lenses. The characteristics of each cell are approximately replaced by the characteristics of the cell center. The theory of dielectric lens can still be used to approximately analyze the metasurface lens. The dual-band focusing characteristic will be verified later.

Based on the above analysis, the dual-band multi-beam design method is summarized. The dual-band planar metasurface lens can obtain a series of same focus positions at both central frequencies. The dual-band planar antenna array can be designed as a feed array, and each antenna element is arranged near the focus position. By exciting the antenna element, the dual-band multi-beam function can be achieved.

To further verify the feasibility of the method, a double-layer dual-band metasurface lens and a five-element dual-band planar antenna array is designed as shown in Figure 1. The dual-band metasurface lens is a double-layer structure composed of dual-band meta-cells. The five-element antenna array consists of five identical dual-band magnetoelectric (ME) dipole antennas with linear arrangement. 13 GHz and 23.5 GHz are selected as the central operating frequencies.

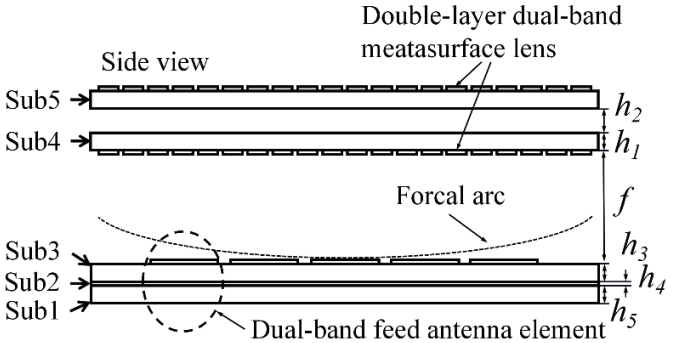

Figure 1. Side view of the lens antenna.

3. METASURFACE LENS DESIGN

3.1. Dual-Band Meta-Cell

In the design of metasurface lens, meta-cells are used for phase compensation. The frequency characteristics of the metasurface lens mainly depend on the meta-cells.

Since the meta-cell have different phase compensation values at two operating frequencies, it is essential to design the meta-cell that the phase can be independently adjusted at each frequency. Figure 2(a) shows the dimensions of the proposed dual-band meta-cell. The single-layer structure consists of a substrate with thickness of h_1 and a copper pattern layer with a thickness of 0.035 mm. The edge part of the copper pattern is a derived Jerusalem cross (JC), which is used to control the phase of the lower frequency band. This structure is adopted because the phase control of JC cell mainly depends on the strip length at the edge of the cell and has little relationship with the strip at the center of the cell. The central part of the copper pattern is a ring and a circular patch to control the phase of the higher frequency band. Similarly, the phase control of the structure only depends on

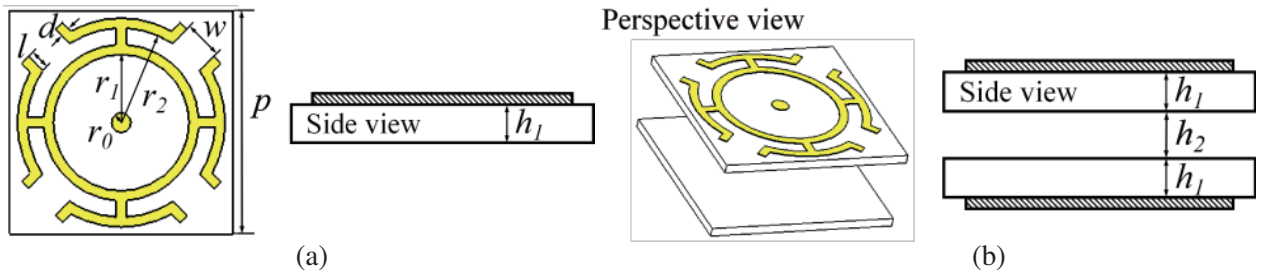

Figure 2. Configuration of the designed dual-band meta-cell. (a) Single layer dual-band meta-cell. $r_0 = 0.6$, $r_1 = 2.9$, $r_2 = 3.8$, $d = 0.4$, $l = 0.8$, $w = 1.0$, $p = 9.0$, $h_1 = 0.406$ and $h_2 = 3.04$, all dimensions are in mm. (b) Double-layer dual-band meta-cell.

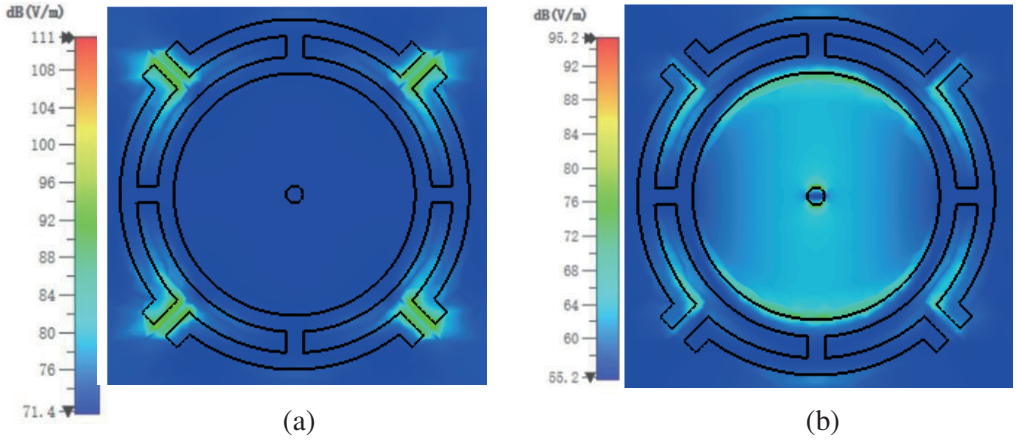

Figure 3. Electric field intensity distribution on the meta-cell. (a) 13 GHz. (b) 23.5 GHz.

the area between the circular patch and the ring. In addition, the ring structure and the attached stubs at the end of the JC edge strip are both conducive to reducing the influence between two bands.

The simulated electric field intensity is shown in Figure 3. The electric fields at 13 GHz and 13.5 GHz are mainly distributed in different areas of the cell, indicating that the performance can be independently changed by changing the dimension of the different areas.

Two identical cells are cascaded as final double-layered cell as shown in Figure 2(b). Cascading more layers of cells will achieve better performance. According to [2], the double-layered cell with maximum phase shift of 240° and the maximum transmission loss of 6.6 dB can reflect the radiation characteristics of the metasurface lens antenna. Therefore, double-layer structure is used to validate the design method. Rogers RO4003C ($\varepsilon_r = 3.55$ and $\tan\delta = 0.0027$) with thickness of 0.203 mm is selected as the substrate in the simulation.

Figure 4 shows the simulated performance with different w, r_0, and r_1. In Figure 4(a) and Figure 4(b), when w changes, the maximum phase shift of 240° at 13 GHz is obtained with a maximum transmission loss of 6.5 dB. The phase shift is always less than 30° at 23.5 GHz. As shown in Figure 4(c) and Figure 4(d), when r_0 and r_1 change, a phase shift of 235° can be obtained at 23.5 GHz with a maximum transmission loss of 6 dB. At the same time, the phase shift at 13 GHz can be guaranteed within 30°. The dual-band meta-cell has relatively independent performance at 13 GHz and 23.5 GHz. By cascading more layers of meta-cells, lower transmission loss can be achieved.

3.2. Metasurface Lens and Focusing Characteristics

A circular aperture lens is designed using dual-band meta-cells. The diameter of circular aperture D is 90 mm. According to [2], $f/D = 0.5$ is applied to ensure a relatively uniform focus distribution.

For single band lens, the phase compensation of cells at different positions can be calculated by

$$\varphi_c = -\frac{2\pi f}{\lambda_0} \cdot \frac{1-\cos(\theta)}{\cos(\theta)} \pm 2n\pi \tag{6}$$

$$\theta = \tan^{-1}(r/f) \tag{7}$$

where r is the distance from the center of the cell to the center of the lens, λ_0 the wavelength in free space at the central frequency, and θ the angle of the incident ray deviating from the axis. According to the analysis in Section 2, the phase compensations of the dual-band lens can also be calculated by (6). For the phase calculation of different frequency bands of the same cell, r, θ and f should be the same. $\lambda_0 = 23.08$ mm and $\lambda_0 = 12.77$ mm are taken, respectively, corresponding to the frequencies of 13 GHz and 23.5 GHz. The distribution of lens phase compensation is shown in Figure 5.

The three-dimensional model of the dual-band lens is built, and focusing characteristics at 13 GHz and 23.5 GHz are simulated. The lens is illuminated by plane waves with incident angles $\alpha = 0°$, 10°, and 20°, respectively. The electric field intensity distributions on the focal plane of the lens are shown in

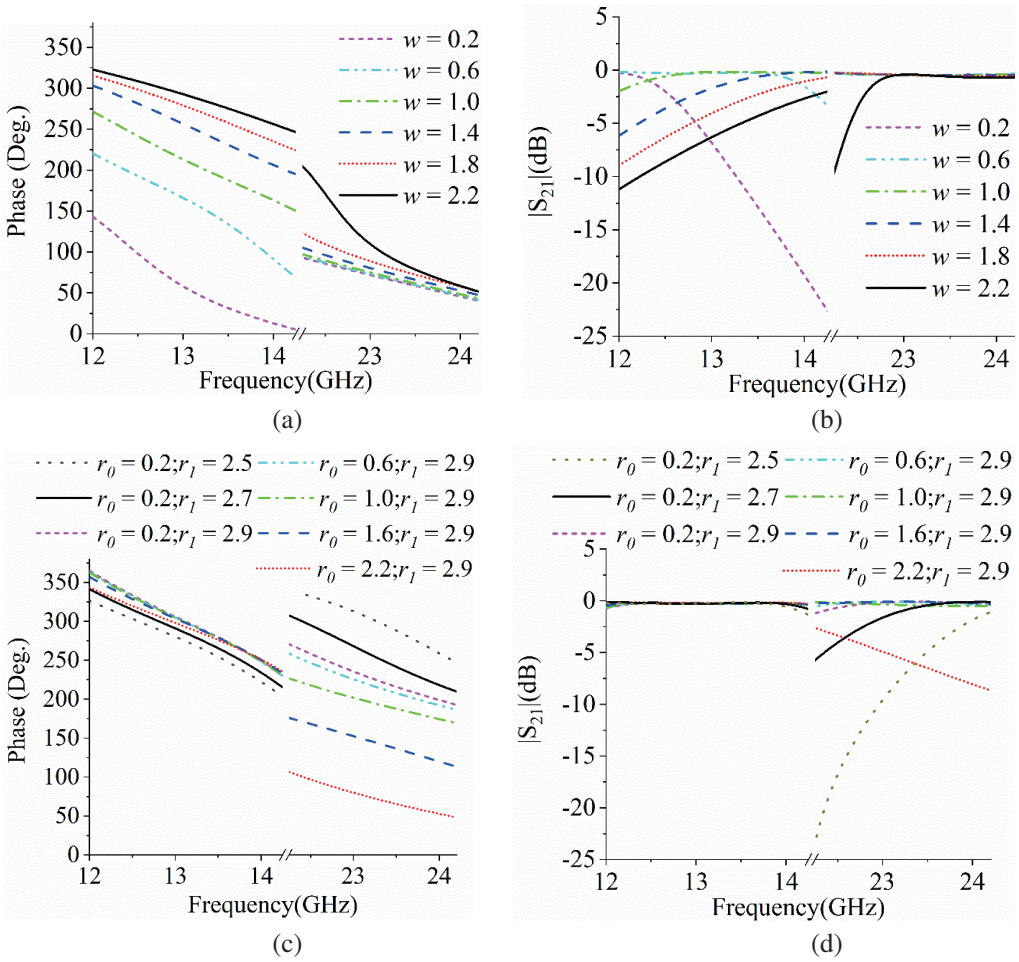

Figure 4. Simulated performances of the designed dual-band meta-cell. (a) Transmission phase with different w. (b) Transmission amplitude with different w. (c) Transmission phase with different r and r_1. (d) Transmission amplitude with different r and r_1.

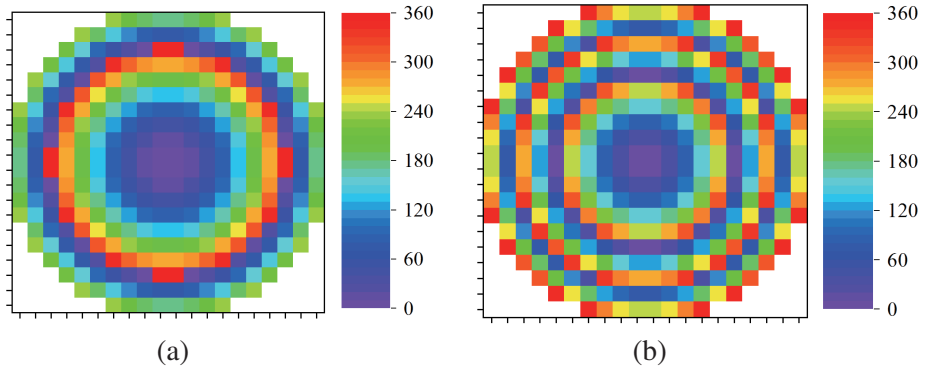

Figure 5. Phase distributions on dual-band metasurface lens. (a) 13 GHz. (b) 23.5 GHz.

Figure 6. The simulated results show that under the plane wave irradiation with incident angles $\alpha = 0°$, 10°, and 20°, the maximum electric field positions at 13 GHz on the focal plane are 0 mm, 19.91 mm, and 38.50 mm away from the focal plane center, respectively, and the maximum electric field positions at 23.5 GHz are 0 mm, 19.87 mm, and 38.5 mm away from the focal plane center, respectively. After the

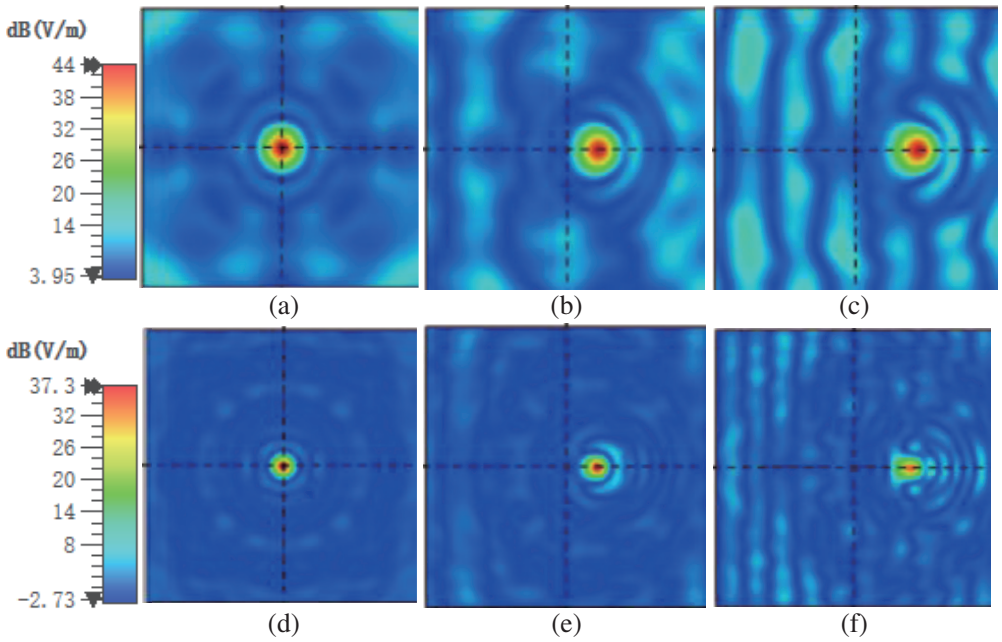

Figure 6. Electric field intensity distributions on focal plane. (a) $\alpha = 0°$ at 13 GHz. (b) $\alpha = 10°$ at 13 GHz. (c) $\alpha = 20°$ at 13 GHz (d) $\alpha = 0°$ at 23.5 GHz. (e) $\alpha = 10°$ at 23.5 GHz. (f) $\alpha = 20°$ at 23.5 GHz.

plane wave passes through the designed dual-band lens, the two considered frequencies have almost the same focusing position under the same incident angle. These focusing positions guide the arrangement of feed antenna elements.

4. FIVE-ELEMENT FEED ANTENNA DESIGN

4.1. Dual-Band Feed Antenna Element

A dual-band ME dipole antenna is designed to form a five-element feed antenna array. The configuration of the antenna is shown in Figure 7. Its mechanism is similar to [21]. The antenna in this paper operates at 13 GHz and 23.5 GHz with a higher frequency ratio, and two rows of metallized blind holes

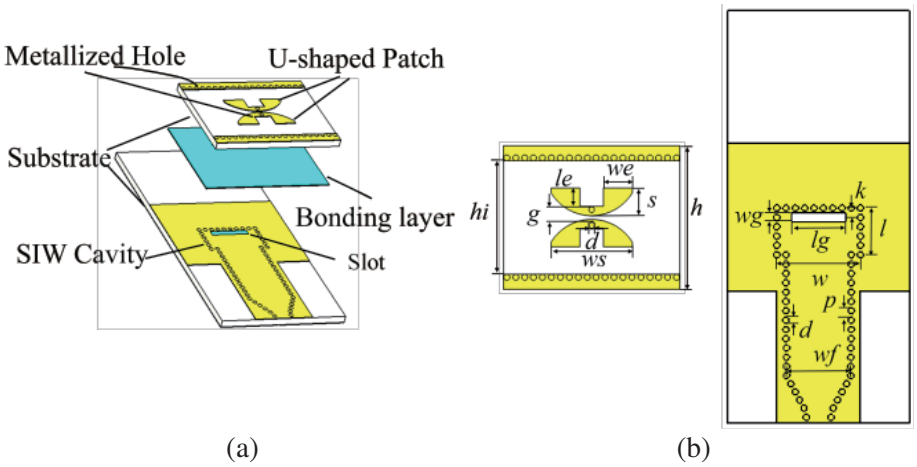

Figure 7. Configuration of the feed antenna element. (a) Configuration of the ME dipole. (b) Patterns on each substrate.

are introduced to adjust the beamwidth of the feed antenna.

The ME dipole consists of two mirrored U-shaped patches, a substrate integrated waveguide (SIW) cavity with slotted top and two metallized vias connecting the patches to the slot. The two mirrored U-shaped patches work as an electric dipole (E-dipole), while the slot on the top of the SIW cavity and two metallized vias work as a magnetic dipole (M-dipole). In the lower frequency band, 0.5λ modes of the E-dipole and M-dipole are excited to form the 0.5λ mode of the ME dipole. In the higher frequency band, 1λ modes of the E-dipole and the M-dipole are excited to form the 1λ mode of the ME dipole. In order to achieve compact configuration and better bandwidths, an SIW cavity is designed to feed the antenna. Metallized blind holes are arranged on both sides of the U-shaped patches on the upper substrate to adjust the lobe width of the feed antenna. In addition, a bonding layer is used to bond the substrates. In order to feed the antenna, a substrate integrated waveguide (SIW)-to-grounded coplanar waveguide (GCPW) transition is designed as shown in Figure 8.

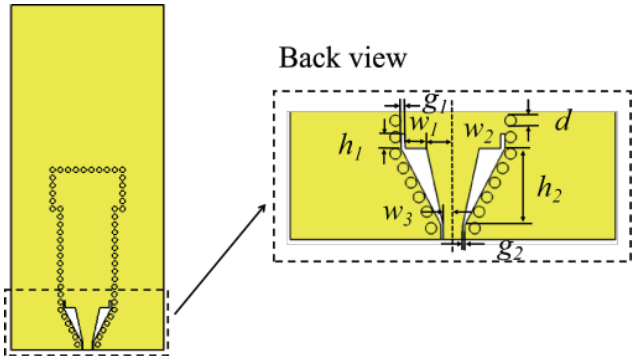

Figure 8. Configuration of the SIW-to-GCPW transition.

The dimensions of the simulated and optimized feed antenna are summarized in Table 1. AGC TLY-5 ($\varepsilon_r = 2.2$ and $\tan\delta = 0.0009$) with a thickness of 0.787 mm is selected as the substrates for simulation. The relative permittivity of the bonding layer is 2.8, and the thickness is 0.114 mm.

Table 1. Parametric value of the feed antenna (unit: millimeter).

PRM.	*we*	*le*	*g*	*ws*	*s*	*d*
Value	2.4	1.5	1.3	6.8	2.3	0.5
PRM.	*hi*	*h*	*wg*	*lg*	*k*	*l*
Value	9.5	12	0.7	4.4	0.73	3.8
PRM.	*w*	*p*	*wf*			
Value	6.82	0.75	5.25			

The simulated $|S_{11}|$ and gains are shown in Figure 9. The impedance bandwidths of the antenna are 12.6–13.7 GHz and 22.3–24.6.8 GHz with the maximum gains of 9.2 dBi and 12 dBi, respectively. The simulated patterns are shown in Figure 10. The lobe widths of E-plane patterns are 44° and 32° at 13 GHz and 23.5 GHz, respectively, and the cross polarization of E-planes is less than −60 dB. The lobe widths of H-plane patterns are 55° and 36° at 13 GHz and 23.5 GHz, respectively, and the cross polarization of H-plane is less than −20 dB. The simulated results show that the feed antenna has good dual-band linear polarization performance.

4.2. Five-Element Feed Antenna Configuration

In order to form multiple beams, five identical feed antenna elements are linearly arranged on the focal plane. The configuration of the dual-band five-element planar antenna array is shown in Figure 11. The

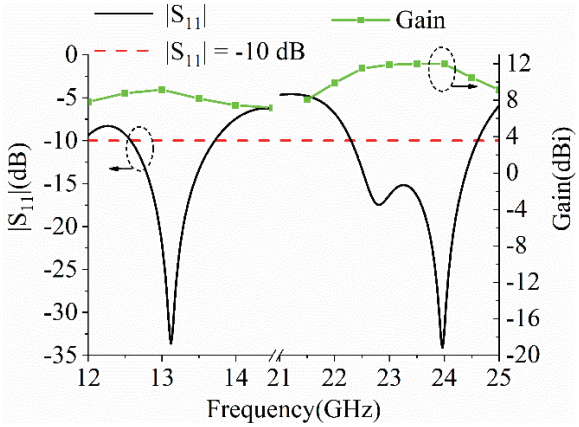

Figure 9. Simulated $|S_{11}|$ and gain of the single feed antenna.

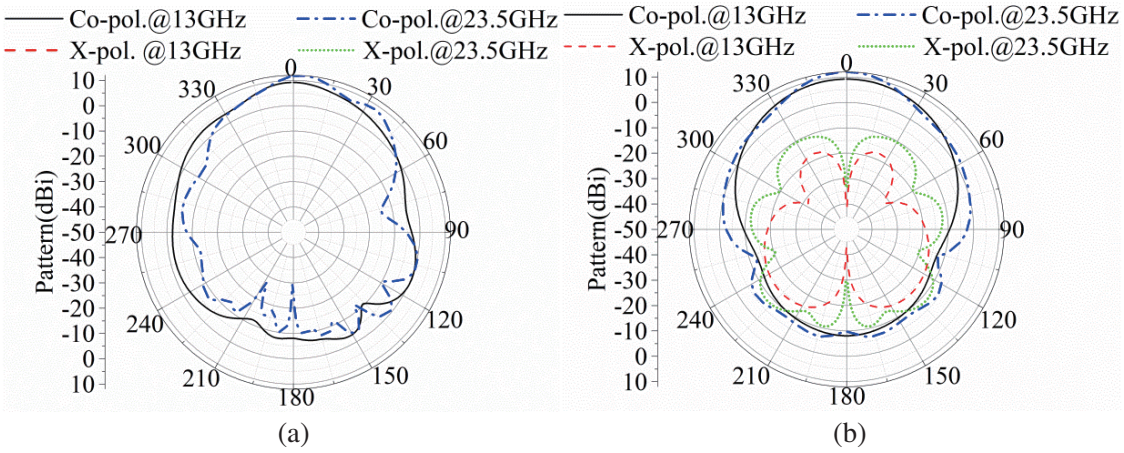

Figure 10. Simulated patterns of the single feed antenna. (a) Patterns in E-plane. (b) Patterns in H-plane.

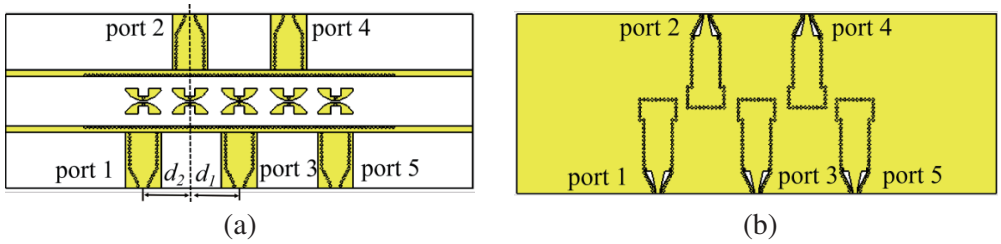

Figure 11. Configuration of five-element feed antenna. (a) Front view. (b) Back view.

five antennas are designed on a planar substrate. For ease of testing, two of the antennas are inverted. The center of each pair of U-shaped patches is on the same line. The feed ports of the five antennas are labeled ports 1–5. The distances from port 2 to port 3 and from port 4 to port 3 are denoted as d_1. The distances from port 1 to port 2 and from port 4 to port 5 are denoted as d_2.

5. SIMULATION, EXPERIMENTS AND DISCUSSIONS

The double-layer dual-band metasurface lens is loaded on a five-element dual-band planar antenna array and simulated. The focus position can roughly indicate the appropriate area of the antenna geometric center. Through simulation and optimization, the distances between feed antennas $d_1 = 19\,\text{mm}$, $d_2 = 40\,\text{mm}$ are obtained. In order to further discuss the feasibility of the design method, The prototype of the lens antenna is fabricated and tested. The photographs of the prototype are shown in Figure 12.

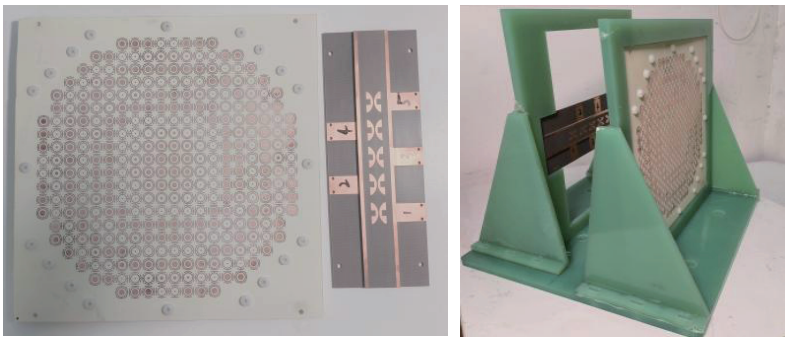

Figure 12. Photograph of dual-band multi-beam antenna.

The lens antenna is axisymmetric, so the simulated and tested results excited by ports 1–3 are displayed. The simulated and measured S-parameters and gains are shown in Figure 13. The simulated impedance bandwidths corresponding to ports 1–3 are 12.7–13.5 GHz, 12.5.1–13.5 GHz, and 12.7–13.5 GHz in the lower frequency band, and 21.7–24.0 GHz, 21.8–24.1 GHz, and 21.9–24.1 GHz in the higher frequency band, respectively. The isolation is larger than 20 dB in both bands. The gains are 16.2–18.3 dBi, 18.2–19.8 dBi, and 18.1–19.9 dBi over the lower frequency band, and 16.5–18.4 dBi, 18.1–19.7 dBi, and 18.2–21.3 dBi over the higher frequency band, respectively. The simulated and measured results are basically consistent.

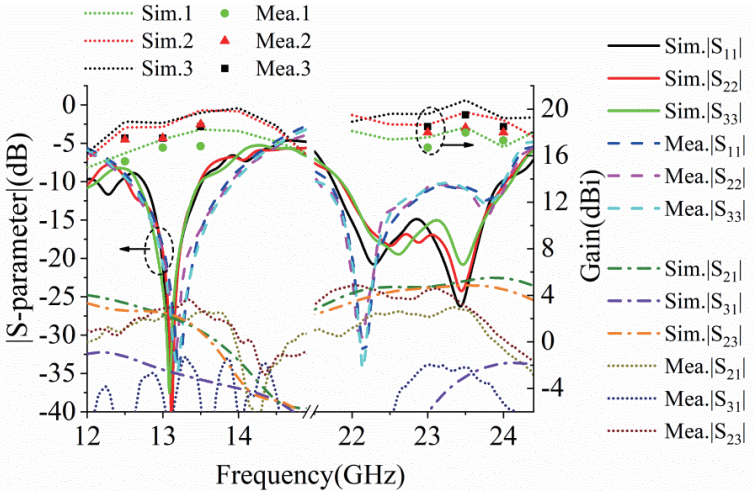

Figure 13. S-parameters and gains of the dual-band multi-beam lens antenna.

The simulated patterns at 13 GHz and 23.5 GHz are shown in Figures 14(a) and (b). The beam directions of the patterns corresponding to ports 1–3 are 20.0°, 10.0°, and 0° at 13 GHz, 18.0°, 9.0°, and 0° at 23.5 GHz, respectively. The beam directions of the same port are slightly different at 13 GHz and 23.5 GHz, which is mainly caused by the fact that the equivalent phase centers of the feed antenna

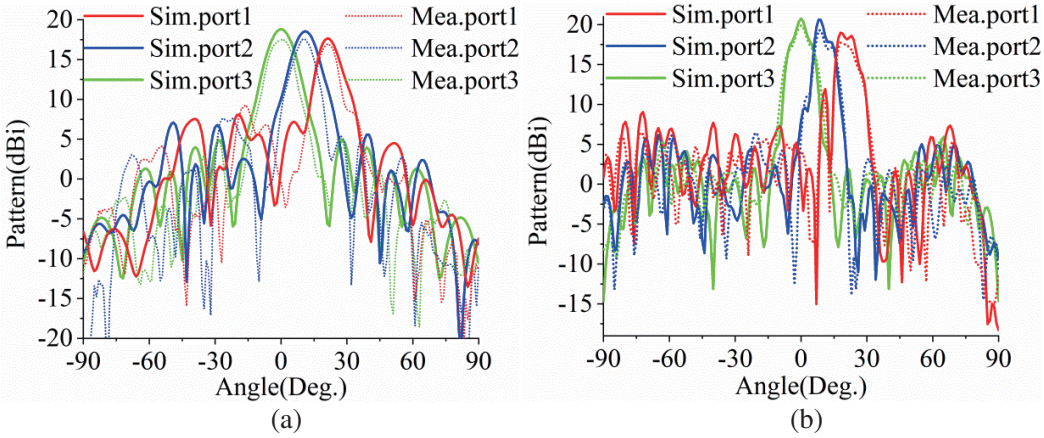

Figure 14. Simulated patterns of the dual-band multi-beam lens antennas excited by port 1–3. (a) Patterns at 13 GHz. (b) Patterns at 23.5 GHz.

do not coincide at 13 GHz and 23.5 GHz. The deterioration of the patterns at 23.5 GHz is caused by inaccurate phase compensation.

The simulated and tested results indicate that the lens antenna generates five independent beams at both 13 GHz and 23.5 GHz, and the dual-band multi-beam function is achieved through the proposed design method. The tested patterns at 23.5 GHz are distorted compared to the 13 GHz results. This is probably due to the defocus caused by machining error of the fabricated prototype.

6. CONCLUSION

A design method for compact dual-band multi-beam antennas is proposed. The dual-band planar metasurface lens can obtain a series of same focus positions at both central frequencies. The dual-band planar antenna array can be designed as a feed array, and each antenna element is arranged near the focus position. By exciting the antenna element, the dual-band multi-beam function can be achieved. Compared with horn antenna used as a dual-band feed to achieve beam scanning, the dual-band multi-beam antenna designed through this method has a compact configuration, low cost, and is easy to integrate with other devices for communication applications.

The dual-band multi-beam function of the antenna by this method has been verified through a double-layer dual-band metasurface lens and a five-element dual-band planar antenna array. A dual-band meta-cell with relatively independent performance at 13 GHz and 23.5 GHz is designed to form the metasurface lens. A dual-band ME dipole antenna is used as the feed antenna element. The simulated and tested results indicate that the lens antenna generates five independent beams at both 13 GHz and 23.5 GHz.

Considering practical applications, the solution to improve antenna performance and reduce losses is suggested. By cascading more layers of meta-cells proposed in this paper, the transmission amplitude and transmission phase performance of the dual-band meta-cells will be greatly improved, and the performance of the dual-band multi-beam antenna will also be significantly improved. Some of the beams pointed at fixed locations are not ideal, which need to be optimized in further work.

This paper provides a reliable design method of dual-band multi-beam antenna. The design method is expected to be applied to 5G frequencies of 26 GHz and 47 GHz and is promising for 5G multibeam applications of wireless communication.

REFERENCES

1. Hong, W., Z. H. Jiang, C. Yu, et al., "Multibeam antenna technologies for 5G wireless communications," *IEEE Trans. Antennas Propag.*, Vol. 65, No. 12, 6231–6249, Dec. 2017.

2. Jiang, M., Z. N. Chen, Y. Zhang, W. Hong, and X. Xuan, "Metamaterial-based thin planar lens antenna for spatial beamforming and multibeam massive MIMO," *IEEE Trans. Antennas Propag.*, Vol. 65, No. 2, 464–472, Feb. 2017.
3. Li, T. and Z. N. Chen, "Control of beam direction for substrate-integrated waveguide slot array antenna using metasurface," *IEEE Trans. Antennas Propag.*, Vol. 66, No. 6, 2862–2869, Jun. 2018.
4. Xue, C., Q. Lou, and Z. N. Chen, "Broadband double-layered Huygens' metasurface lens antenna for 5G millimeter-wave systems," *IEEE Trans. Antennas Propag.*, Vol. 68, No. 3, 1468–1476, Mar. 2020.
5. Wang, H.-F., Z.-B. Wang, Z.-H. Wu, and Y.-R. Zhang, "Beam-scanning lens antenna based on elliptical paraboloid phase distribution metasurfaces," *IEEE Trans. Antennas Propag.*, Vol. 18, No. 8, 1562–1566, Aug. 2019.
6. Singh, A. K., M. P. Abegaonkar, and S. K. Koul, "Wide angle beam steerable high gain flat top beam antenna using graded index metasurface lens," *IEEE Trans. Antennas Propag.*, Vol. 67, No. 10, 6334–6343, Oct. 2019.
7. Su, Y. and Z. N. Chen, "A flat dual-polarized transformation-optics beamscanning luneburg lens antenna using PCB-stacked gradient index metamaterials," *IEEE Trans. Antennas Propag.*, Vol. 66, No. 10, 5088–5097, Oct. 2018.
8. Su, Y. and Z. N. Chen, "A radial transformation-optics mapping for flat ultra-wide-angle dual-polarized stacked GRIN MTM luneburg lens antenna," *IEEE Trans. Antennas Propag.*, Vol. 67, No. 5, 2961–2970, May 2019.
9. Li, T. and Z. N. Chen, "Compact wideband wide-angle polarization-free metasurface lens antenna array for multibeam base stations," *IEEE Trans. Antennas Propag.*, Vol. 68, No. 3, 1378–1388, Mar. 2020.
10. Li, S., Z. N. Chen, T. Li, F. H. Lin, and X. Yin, "Characterization of metasurface lens antenna for sub-6 GHz dual-polarization full-dimension massive MIMO and multibeam systems," *IEEE Trans. Antennas Propag.*, Vol. 68, No. 3, 1366–1377, Mar. 2020.
11. Katare, K. K., S. Chandravanshi, A. Biswas and M. J. Akhtar, "Realization of split beam antenna using transmission-type coding metasurface and planar lens," *IEEE Trans. Antennas Propag.*, Vol. 67, No. 4, 2074–2084, Apr. 2019.
12. Li, H., et al., "Wide-angle beam steering based on an active conformal metasurface lens," *IEEE Access*, Vol. 7, 185264–185272, 2019.
13. Cai, T., G.-M. Wang, J.-G. Liang, Y.-Q. Zhuang, and T.-J. Li, "High-performance transmissive meta-surface for C-/X-band lens antenna application," *IEEE Trans. Antennas Propag.*, Vol. 65, No. 7, 3598–3606, Jul. 2017.
14. Aziz, A., F. Yang, S. Xu, and M. Li, "An efficient dual-band orthogonally polarized transmitarray design using three-dipole elements," *IEEE Antennas Wireless Propag. Lett.*, Vol. 17, No. 2, 319–322, Feb. 2018.
15. Aziz, A., F. Yang, S. Xu, M. Li, and H.-T. Chen, "A high-gain dual-band and dual-polarized transmitarray using novel loop elements," *IEEE Antennas Wireless Propag. Lett.*, Vol. 18, No. 6, 1213–1217, Jun. 2019.
16. Cai, M., Z. Yan, F. Fan, S. Yang, and X. Li, "Double-layer Ku/K dual-band orthogonally polarized high-efficiency transmitarray antenna," *IEEE Access*, Vol. 9, 89143–89149, 2021.
17. Pham, T. K., L. Guang, D. González-Ovejero, and R. Sauleau, "Dual-band transmitarray with low scan loss for satcom applications," *IEEE Trans. Antennas Propag.*, Vol. 69, No. 3, 1775–1780, Mar. 2021.
18. Madi, R., A. Clemente, and R. Sauleau, "Dual-band, dual-linearly polarized transmitarrays for SATCOM applications at Ka-band," *2022 16th Europ. Conf. Antennas Propag. (EuCAP 2022)*, 1–4, Madrid, Spain, 2022.
19. Wang, P., W. Ren, Q. Zeng, Z. Xue, and W. Li, "Dual-band beam-scanning antenna at ka-band by rotation of two transmitarrays," *IEEE Antennas Wireless Propag. Lett.*, Vol. 21, No. 9, 1792–1796, Sept. 2022.

20. Zeng, Q., Z. Xue, W. Ren, and W. Li, "Dual-band beam-scanning antenna using rotatable planar phase gradient transmitarrays," *IEEE Trans. Antennas Propag.*, Vol. 68, No. 6, 5021–5026, Jun. 2020.
21. Ni, S., X. Li, X. Qiao, Q. Wang, and J. Zhang, "A compact dual-wideband magnetoelectric dipole antenna for 5G millimeter-wave applications," *IEEE Trans. Antennas Propag.*, Vol. 70, No. 10, 9112–9119, Oct. 2022.
22. Li, H., G. Wang, X. Gao J. Liang, and H. Hou, "An X/Ku-band focusing anisotropic metasurface for low cross-polarization lens antenna application," *Progress In Electromagnetics Research*, Vol. 159, 79–91, 2017.